CarakaTani
Journal of Sustainable Agriculture
ISSN 2613-9456 (Print) 2599-2570 (Online)

Caraka Tani: Journal of Sustainable Agriculture, 41(2), 285-304, 2026
URL: https://jurnal.uns.ac.id/carakatani/article/view/106618
DOI: http://dx.doi.org/10.20961/carakatani.v41i2.106618

Development of an Edible Tray Composed of Potato Peel Starch and Coffee Pulp Fiber

José Arroyo-Villanueva[1], Gloria Muñoz-Villalobos[1], Raúl Siche[1], Roberto Chuquilín-Goicochea[2,3]*, Luz Quispe-Sanchez[3], Haley Figueroa-Avalos[1] and Carmen Marín-Tello[4]

[1]Escuela de Ingeniería Agroindustrial, Facultad de Ciencias Agropecuarias, Universidad Nacional de Trujillo, Trujillo, Peru; [2]Universidad Privada del Norte, Lima, Peru; [3]Grupo de Investigación en biopolímeros, Instituto de Investigación para el Desarrollo Sustentable de Ceja de Selva, Universidad Nacional Toribio Rodríguez de Mendoza de Amazonas, Chachapoyas, Peru; [4]Laboratorio de Investigaciones sobre Fisiología y Metabolismo Nutricional, Departamento de Farmacología, Facultad de Farmacia y Bioquímica, Universidad Nacional de Trujillo, Trujillo, Peru

*Corresponding author: roberto.chuquilin@upn.edu.pe

Abstract

Reducing plastic pollution and combating childhood anemia–which affects over 38.6% of Peruvian children–require sustainable, nutrient-rich alternatives. This study developed iron-fortified edible trays using potato peel starch (PPS), potato peel flour (PPF), and coffee pulp fiber (CPF), an agro-industrial waste containing 44 to 57 mg kg^{-1} of iron. Using an experimental design with 9 treatments and a control, 2 series were conducted using coarse (CPF-CT) and thin (CPF-TT) fiber. Physical (color, water absorption, and density) and mechanical (tensile and compressive strength) properties were evaluated via analysis of variance (ANOVA), Dunnett's test, multiple linear regression, Pareto diagram, and principal component analysis (PCA). PCA revealed a critical trade-off between mechanical strength and impermeability, identifying an "optimal packing" zone at 10% CPF-TT, where fiber efficiently fills matrix voids. Consequently, formulations with 2.5% CPF-CT and 7.5% CPF-TT were selected as the most balanced candidates. These samples underwent subsequent Fourier-transform infrared spectroscopy (FTIR), scanning electron microscopy (SEM), and nutritional analysis. The formulation containing 50 g PPS, 15 g PPF, and 7.5 g CPF-TT exhibited the highest iron bioaccessibility. These results demonstrate the potential of coffee pulp-reinforced trays as a promising functional packaging solution to address both environmental waste and public health challenges.

Keywords: bioaccessibility; biodegradable; coffee pulp; edible tray; native starch

Cite this as: Arroyo-Villanueva, J., Muñoz-Villalobos, G., Siche, R., Chuquilín-Goicochea, R., Quispe-Sanchez, L., Figueroa-Avalos, H., & Marín-Tello, C. (2026). Development of an Edible Tray Composed of Potato Peel Starch and Coffee Pulp Fiber. *Caraka Tani: Journal of Sustainable Agriculture*, *41*(2), 285-304. doi: http://dx.doi.org/10.20961/carakatani.v41i2.106618

INTRODUCTION

The growing environmental problem caused by food containers has reached a critical level, pushing governments to take strong action to restrict their use (Rondon-Jara et al., 2020). Producing food trays not only involves excessive use of resources such as water, non-renewable energy, chemicals, wood, and fiber (Elfaleh et al., 2023) but also generates wastewater containing toxic substances (Chen et al., 2021). Plastic waste also threatens marine life and birds (Mao et al., 2020; Wang et al., 2020; Zhang et al., 2020). To address this situation, the need for more sustainable and ecological alternatives arises, and it is here that biopolymers present themselves as a viable option (Habibi et al., 2020).

Peru, with 6 million tons of production in 2022, a cultivated area of 340.9 thousand hectares, and an average yield of 17.6 tons ha^{-1}, leads potato

* *Received for publication July 22, 2025*
Accepted after corrections May 4, 2026

production in Latin America. Approximately 90% of this production comes from the Peruvian highlands, where native varieties of great importance, such as the "Huevo de Indio" variety, are preserved and cultivated (Ayala et al., 2025).

Coffee pulp represents 40% of the total weight of the fruit; it is rich in iron, magnesium, zinc, and other underutilized nutrients (Vallejos-Jiménez et al., 2025). Additionally, agroindustrial residues contain starch and fiber, making them a potential source of raw material for the elaboration of biodegradable trays through thermoforming. Integrating coffee pulp-derived compounds, specifically caffeic acid, promotes the microbiological stability of food packaging through the inhibition of multidrug-resistant pathogens such as *Vibrio cholerae* (Rawangkan et al., 2022). Furthermore, these extracts exhibit antimicrobial efficacy in preventing dental caries (Bollamma et al., 2023).

Edible trays made from agro-industrial waste are not only an environmentally friendly solution to the large amount of waste, but could also help combat childhood anemia. It is a significant public health issue in Peru, where 38.6% of children under 3 years old are anemic, mainly due to insufficient iron intake (Tokumura and Mejía, 2023). These edible trays can be obtained through thermoforming, which allows for the gelatinization of starch and the formation of a foamy structure with good physical and mechanical properties (Dybka-Stępień et al., 2021). The addition of coffee pulp fiber and other additives can lead to higher-quality trays (Cruz-Tirado et al., 2020).

Rigid edible trays are an innovative and sustainable alternative: they not only protect the food they contain, but being edible, they can be consumed along with it, thus reducing waste. Recent studies have developed edible films with antioxidant, antimicrobial, and anticancer properties, allowing for a better shelf life of food (Oliveira Filho and Egea, 2022). However, the development of edible trays from agro-industrial waste is still limited, and the impact of incorporating fiber can be unfavorable for their physical and mechanical properties, but it presents significant potential for future innovations (Mohareb and Mittal, 2007; Patel, 2019).

Starch is versatile for developing "green packaging"; however, on its own, it presents limitations in terms of mechanical properties and hygroscopicity. The addition of lignocellulosic waste (such as sugarcane bagasse, corn husks, malt bagasse, and orange peel, among others) improves mechanical and barrier properties, producing packaging with greater rigidity and accelerated biodegradability (Sampaio et al., 2020; Quispe-Sanchez et al., 2025).

Based on this background, edible packaging obtained from a mixture of starch and lignocellulosic waste represents a significant contribution with far-reaching implications for the food industry, because it allows for 2 outcomes: additional use of the packaging before its disposal and the introduction of active substances with nutraceutical applications (Leya et al., 2024). However, insufficient information on machinery, compositions, application techniques, and the analysis of the physio-mechanical properties of edible packaging could be complex, and further research is needed (Devidas Meshram et al., 2023). This study aimed to evaluate the appropriate proportions of starch and fiber from potato peel and coffee pulp to produce edible trays fortified with iron. These trays possess convenient mechanical properties and high bioaccessibility to iron, thereby contributing to environmental sustainability and improving children's health in Peru.

MATERIALS AND METHOD

Materials

Potato peel from the "Huevo de Indio" variety was used in this study as a source of starch and fiber. This variety is among the most commercial native potato varieties from the Peruvian highlands and grows between 2,800 and 4,000 m above sea level, from the La Libertad to Junín regions. It presents high starch content (22.15 to 23.03 g 100 g^{-1}), bioactive compounds such as anthocyanins (4.88 to 17.49 mg cyanidin-3-glucoside 100 g^{-1}) and phenolic compounds (90.47 to 258.32 mg GAE 100 g^{-1}), and antioxidant activity (77.23 to 179.47 µmol TE 100 g^{-1} dry weight) (Bardales et al., 2022). Coffee pulp from the Catimor-Colombia variety was also used, sampled between August and September 2020 in Lonya Grande, Amazonas (78°25'19.2" W, 6°05'42" S), at altitudes between 1,400 and 1,600 m above sea level. It was used as a source of fiber and iron.

Obtention of coffee pulp fiber (CPF)

Coffee cherries were pulped using a food-grade surgical steel pulper. The pulp was then immediately washed and placed in a previously standardized solar tent dryer for 7 days. It was then processed using an electric spice grinder (GRT-20B), followed by Tyler sieves #20 and

#200 (> 850 and < 75 µm, respectively). The 2 flours obtained were labeled "Coarse" (#20–C; CPF-CT) and "Thin" (#200–T; CPF-TT).

Extraction of potato peel starch (PPS)

About 20 kg of potato peel were washed with tap water, then cut into 1 cm × 1 cm pieces. Starch was extracted following a modified protocol by Moustafa et al. (2021): the potato peel square pieces were submerged in 1:1 tap water and sodium bisulfite up to 0.075 g l^{-1}, then homogenized using an industrial blender (Metal Mecánica Agroindustria, Peru) at 3 g for 3 minutes, and filtered using a metal strainer and a muslin cloth. All the filtrate water was then decanted for 15 hours, and the starch obtained was dried in an oven (UF55 Plus, Memmert, Germany) for 48 hours at 40 °C. The resulting dried starch was collected, ground, sieved (Tyler #200), placed in a sealed 1 kg glass jar, and stored in a dry place until further use.

Obtention of potato peel flour (PPF)

PPF was obtained following a modified method by Akter et al. (2023): the residue from the starch extraction was dried in an oven (UF55 Plus, Memmert, Germany) at 40 °C for 24 hours. It was then collected, ground to a fine powder (Tyler #200), and kept in a 1 kg glass jar, then stored in a dry place until further use.

Edible tray formulation and production

Edible trays were obtained from the following 3 ingredients: CPF, PPS, and PPF (Figure 1). The experiment included 18 formulations and a control, with constant temperature and pressure parameters during the thermopressing (Cruz-Tirado et al., 2020). Two particle sizes of CPF were tested, thus obtaining 9 formulations (#200 T and #20 C) as shown in Table 1. Additionally, 1 ml of vanilla and 10 ml of water were added to each formulation.

The edible trays were produced following Cruz-Tirado et al. (2020). The homogenization process was carried out in an industrial blender. Then 60±2 g of the mixture was set in the center of a Teflon cast (27 cm × 20 cm, 3.0 mm thick) in the thermopress (RELES, Lima, Peru) at 150 °C for 10 minutes under 60 bar. The tray was unmolded while still hot and left to cool down at room temperature (25±1 °C). The trays were covered with aluminum foil and stored at room temperature until further characterization.

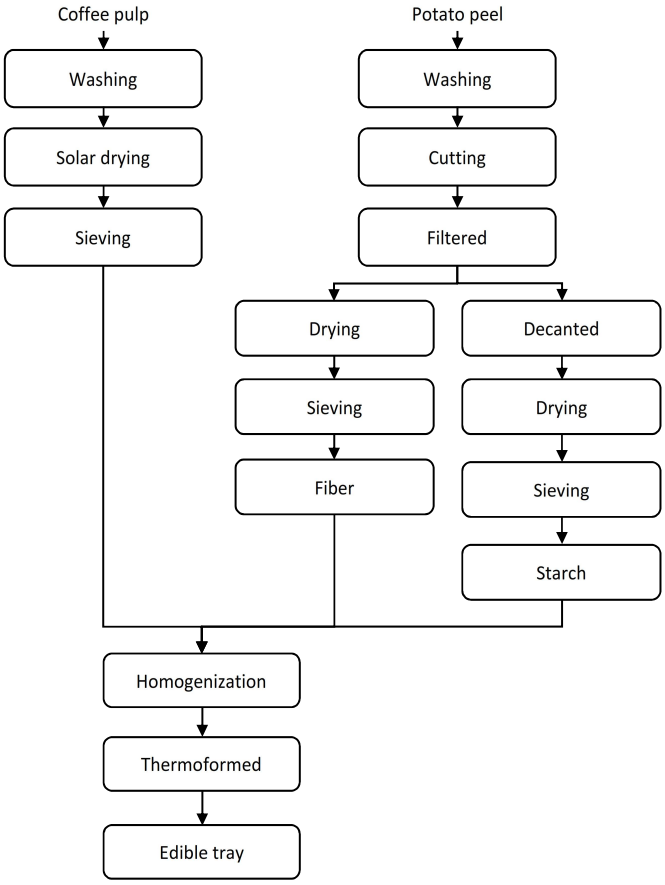

Figure 1. Edible trays production flowchart

Physicochemical characterization of starch and fiber

Chemical analysis

Moisture, ash, protein, fat, and fiber of the PPF were determined according to AOAC (2019) methods. Total carbohydrate content was calculated by subtracting moisture, ash, protein, fat, and fiber from 100 (Collazos et al., 1996).

Swelling power and solubility

The swelling power and solubility of starch were determined using 2% (w/v) starch suspensions in triplicate, as described by Alvis et al. (2008). The suspensions were treated for 30 minutes at 60, 70, 80, and 90 °C using a water bath (Memmert, 2019). Each suspension was centrifuged at 3,030 rpm for 30 minutes (Heraeus Sepatech Labofuge 200, SpectraLab Scientific Inc., Canada). Both pellets and supernatants were weighed, then dried in an oven (Memmert) at 50 °C for 2 days, and weighed again using Equations 1 and 2, respectively.

Amylose and amylopectin determination

Amylose and amylopectin contents were determined following Morrison and Laignelet (1983), for the colorimetric determination of amylose as its blue polyiodide complex.

Edible tray physicochemical characterization

Tensile and compression tests

Tensile and compression tests were performed in triplicate following Bergel et al. (2018) with modifications, using a texture analyzer (TA.HD plus, Stable Micro system, Surrey, UK). The tensile strength was assessed on 100 mm × 20 mm strips, with an initial gripping distance of 15 mm, at a speed of 0.5 mm s^{-1} using the A/HDG probe. The compression test was performed on 50 mm × 30 mm rectangular samples, using a 100 kg load cell to which a P/0.5S stainless steel spherical probe was fixed, at a speed of 1 mm s^{-1}.

Colorimetry

The trays were tested for lightness (L*), a*, b*, and total difference in color (ΔE) using a colorimeter (JZ-300, Kingwell Shenzhen Co., China) in quadruplicate. The ΔE was calculated using Equation 3.

Thickness and density

The method used was as reported in Kahvand and Fasihi (2020), with modifications. The tray thickness was determined using a vernier caliper, and the density (g cm^{-3}) was calculated from the mass (g) and volume (cm^3) of each 100 mm × 25 mm strip, in triplicate.

Moisture and water absorption

Moisture was determined using the gravimetric method in an oven, as described by Namphonsane et al. (2023). Water absorption was determined by weighing a tray sample before submersion in water (M1) and after submersion at 25±1 °C for 30 seconds, then draining the excess water for 5 minutes (M2) (Osorio Mora et al., 2014). Equation 4 was used to calculate water absorption.

Guillotine test

A cutting test was performed as described by Bergel et al. (2018) with modifications, using

Table 1. Edible tray formulations

Treatment	PPS	PPF	CPF	Water (ml)
T0	65	0	0.0	50
T1	60	5	2.5	50
T2	60	5	7.5	50
T3	60	5	10.0	50
T4	55	10	2.5	50
T5	55	10	7.5	50
T6	55	10	10.0	50
T7	50	15	2.5	50
T8	50	15	7.5	50
T9	50	15	10.0	50

Note: PPS = Potato peel starch; PPF = Potato peel flour; CPF = Coffee pulp fiber

$$\text{Swelling Power}\left(\text{g } H_2O/\text{g starch}\right)=\frac{\text{Pellet weight-Starch weight}}{\text{Starch weight}} \quad (1)$$

$$\text{Solubility (\%)}=\frac{\text{Dried supernatant weight}}{\text{Starch weight}}\times 100 \quad (2)$$

$$\Delta E=\sqrt{(L-L^*)^2+(a-a^*)^2+(b-b^*)^2} \quad (3)$$

Where, L*, a*, and b* are the values of the color parameters of the sample.

$$\text{Water absorption capacity (\%)}=\frac{M2-M1}{M1}\times 100 \quad (4)$$

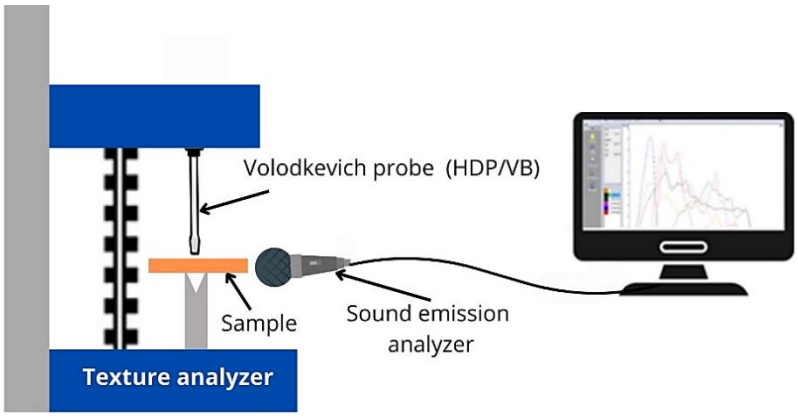

Figure 2. Biting simulation test diagram

a texture analyzer (TA.HD Plus, Stable Micro System, Surrey, UK) with a 5 kg load cell. Firmness was determined on 50 mm × 50 mm samples, at a speed of 1.5 mm s^{-1} using the HDP/BSV probe and 50% deformation.

Biting simulation test

The biting simulation test was performed following Olivera and Salvadori (2011), with modifications, using a texture analyzer (TA.HD Plus, Stable Micro System, Surrey, UK) and a Voldkevich probe (HDP/VB) (Figure 2) attached to a 50 N load cell. The test was conducted on uniform samples measuring 1 mm × 4 mm, at a speed of 2 mm s^{-1} and a depth of 2 mm.

Nutritional value of the tray

Moisture, protein, ash, fat, iron, and carbohydrate were determined following AOAC (2019).

Iron bioaccessibility test

This test was performed at the Centro Público de Investigación CONACYT, Jalisco, Mexico. Bioaccessibility refers to the proportion of a substance that is released from the food matrix and becomes potentially available for absorption during digestion (Rodrigues et al., 2022). For this test, digestions were performed in triplicate in an artificial mouth, stomach, and small intestine.

Infrared spectrophotometry (FTIR)

The wavenumber range on the spectrophotometer (IRPrestige-21, Shimadzu, Kyoto, Japan) was set between 1,000 and 4,000 cm^{-1}, to analyze samples measuring 2.5 mm × 2.5 mm × 0.25 mm (height × width × thickness). A total of 32 reflectance scans per spectrum were performed with a resolution of 4 cm^{-1}. The spectra that were obtained with the ATR-FTIR accessory were corrected and analyzed using OMNIC Spectra Material Characterization Advanced Analysis software (Thermo Scientific).

Scanning electron microscopy (SEM)

All analyses were performed on a SEM (TESCAN, VEGA-3-LMU, Czech Republic). All trays were kept at 25 °C and 60% relative humidity before being prepared for observation of their transversal section. The tray samples were mounted in bronze stubs for viewing of the cross-section. The surfaces were coated with gold to a thickness of 40 to 50 nm. The acceleration voltage was 20 kV for all samples.

Statistical analysis

The analysis of variance (ANOVA) was performed using a completely randomized design in MS-Excel. When the ANOVA was significant, the Dunnett's test was applied to compare the samples to the control. Student's t-tests were used for the 2 final samples. Subsequently, a multiple linear regression analysis was applied, using PPS, PPF, and CPF as independent variables, and their respective ANOVA were performed at the 0.05 significance level. A principal component analysis (PCA) was also applied. These analyses were performed separately for edible trays with CPF-CT and CPF-TT. The software used included MS Excel, Minitab 19, and Matlab.

RESULTS AND DISCUSSION

Characterization of the PPS

Ash content was 2.56±0.01%, similar to the ash content reported for other vegetal starches (Abera et al., 2019). Protein content varied around 1.21±0.01%, affecting viscosity and the ability to form foam inside the tray (Martínez et al., 2022). Fat content was 0.29±0.02%. The carbohydrate content was 95.73±0.02%, slightly lower than that reported for similar plants. This value is associated with the carbohydrate composition, with a fiber content of 3.18±0.09% and an acidity of 0.04±0.00% (expressed as % sulfuric acid per 100 g). Amylose and amylopectin contents were

18.65±0.98% and 81.35±0.98%, respectively. This proportion of amylose to amylopectin contents indicates that PPS displays a higher water-retention capacity and a smoother texture for uses requiring good gelation and stability (Khan et al., 2024).

In the CPF, the carbohydrate content was 56.62±1.74%, fiber 16.94±0.99%, protein 8.53±0.57%, fat 0.69±0.02%, and ash 7.61±0.09%. These values are consistent with those reported by Duangjai et al. (2016). Regarding the composition of PPF, an ash content of 4.22±0.17%, protein 6.97±0.24%, fat 1.77±0.08%, carbohydrates 76.17±1.04%, fiber 1.51±0.03%, and a moisture content of 9.37±0.35% were obtained.

Solubility and swelling power

Solubility and swelling power values (Figure 3) grew with temperature; at 90 °C, the PPS displayed the highest swelling power and solubility values: 27.56±0.41 g g^{-1} and 4.29±0.40%, respectively. This observation suggests that swelling power and solubility in water increase as temperature rises. The relationship with temperature is more noticeable with swelling power, whereas solubility increases gradually (Lin et al., 2020). Starch solubility is mainly associated with amylose dissolution in water after heating, or gelation (Aguirre et al., 2023).

Texture

When tensile strength was tested, C trays (particle size #20) showed an indirect correlation between tensile strength and CPF content (Figure 4), which can be explained by the higher fiber content (Charles et al., 2017). This relation was not observed in T trays (particle size #200). The control treatment showed the highest tensile strength value; when compared to the others, CT4 and CT7 showed values similar to the control. However, TT8 was similar to the control treatment, but CT6 was much higher than the control and considered an atypical value. Starch content also directly correlated to the tension on C treatments, due to higher starch incorporation leading to more compact and homogenous structures (Cruz-Tirado et al., 2017). During the compression test (Table 3), the control showed the highest value (3.37±0.41 kgf), which was significantly superior to all other treatments (C and T). In both C and T treatments, the compression directly correlated to starch content. On the other hand, compression showed an indirect correlation with potato peel and CPF contents. Treatments with high compression values–such as 1.99±0.45 kgf (CT4) and 2.62±0.19 kgf (TT7)–are expected to better resist physical damage, such as crushing.

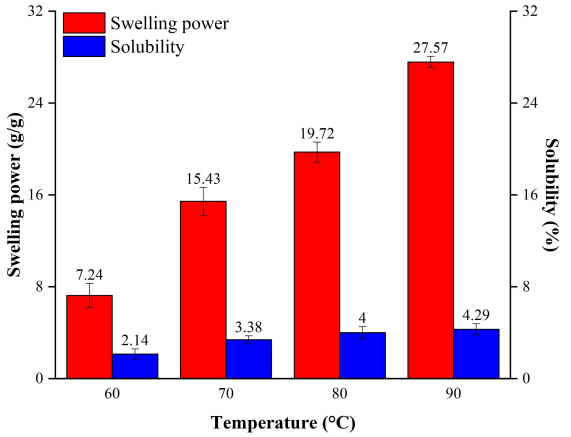

Figure 3. PPS swelling power and solubility
Note: Same columns with different indices are significantly different ($p > 0.05$)

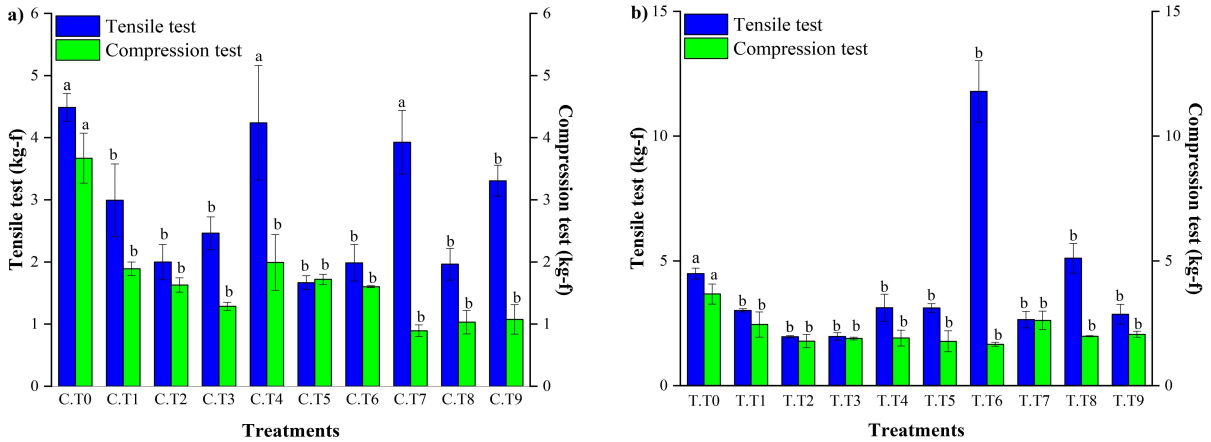

Figure 4. Edible tray mechanical properties: a) CT: Tyler #20; b) TT: Tyler #200
Note: T0 = Control. [a, b] Different letters indicate a significant difference (Dunnett)

Color

Color measurement is a key and widely used parameter in the food industry for quality control (Pandiselvam et al., 2023). The different treatments had an impact on the final product color (Figure 5). Starch content correlated directly with L* and ΔE in both C and T treatments. However, they correlated indirectly with a* and b* (Figure 6). The white color of the starch may have influenced the L* of the trays (Figure 6) (Wrolstad and Smith, 2017).

Physical properties

The thickness of C treatment trays varied between 2.22±0.01 and 2.62±0.02 mm, whereas the thickness of T treatment trays varied between 2.10±0.01 and 3.12±0.15 mm (Figure 7). A similar thickness range (2.57 to 2.60 mm) was reported for trays made from oca starch, sugarcane bagasse fiber, and asparagus peel (Cruz-Tirado et al., 2017). Engel et al. (2021) reported that trays produced from two cassava residues and starch biocomposites were thicker (2.90 to 3.30 mm).

Evidence showed that thickness directly correlated with starch content but indirectly correlated with potato peel and CPF contents. C treatments showed a wider thickness range than T treatments, due to larger particles and

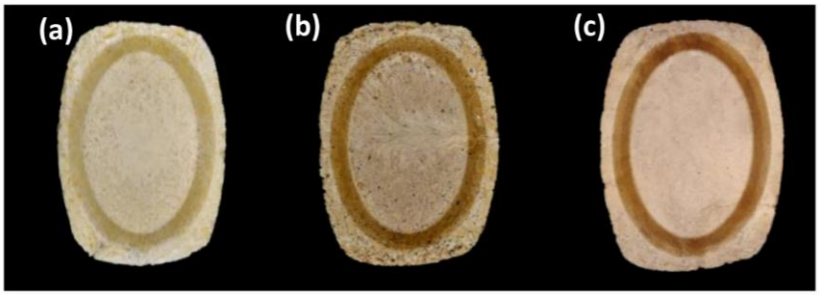

Figure 5. Tray color: (a) T0, (b) CT2, (c) TT3

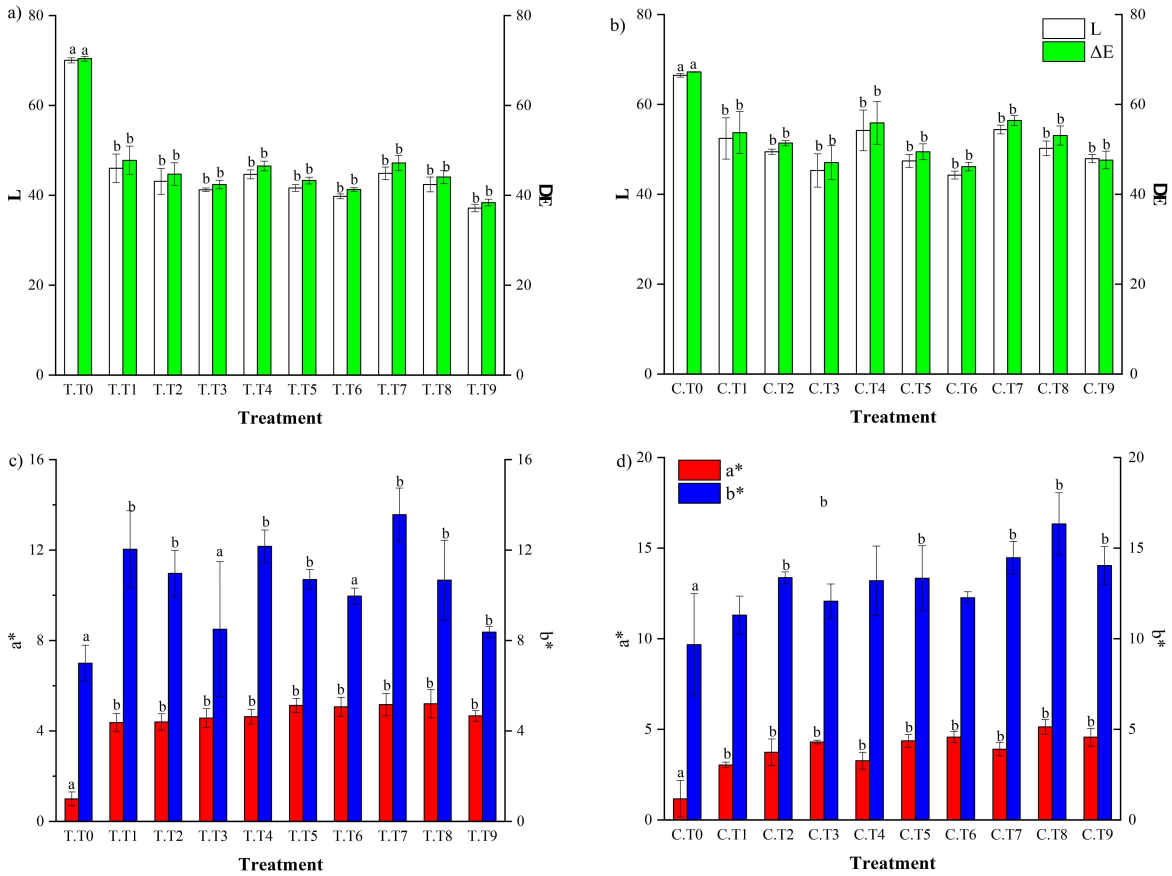

Figure 6. Tray colorimetry properties. a) and b): TT = Tyler #200, c) and d): CT = Tyler #20
Note: T0 = Control. [a, b] Different letters indicate a significant difference (Dunnett)

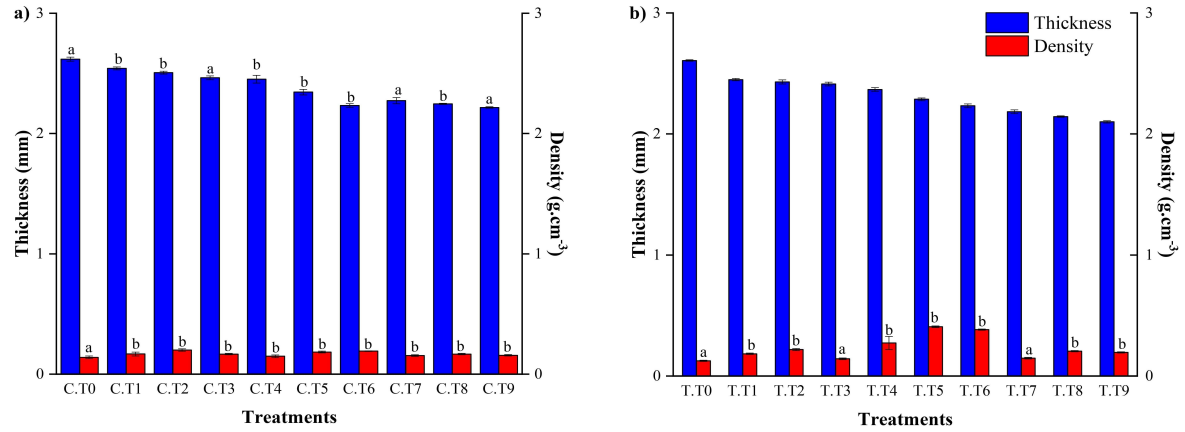

Figure 7. Tray thickness and density. a) CT = Tyler #20; b) TT = Tyler #200
Note: T0 = Control. [a, b] Different letters indicate a significant difference (Dunnett)

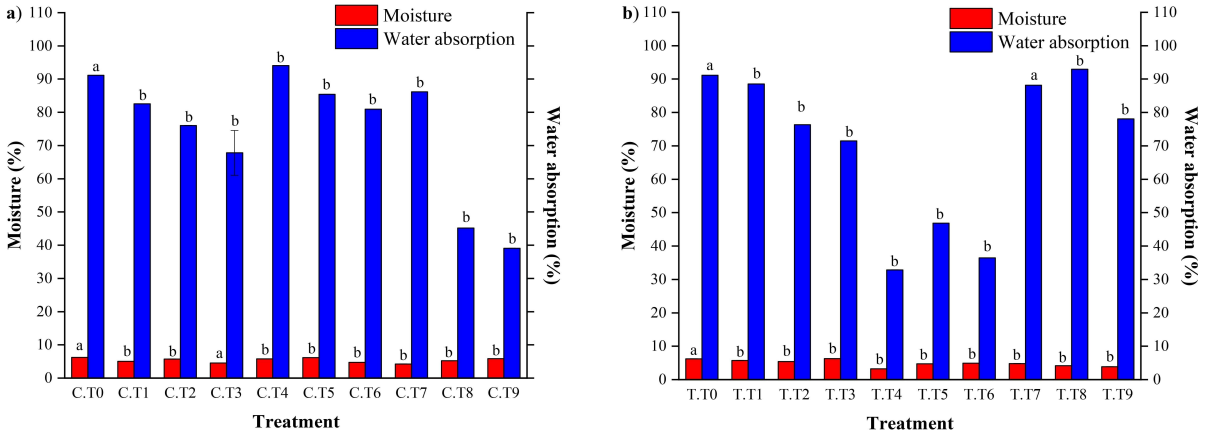

Figure 8. Tray moisture and water absorption. a) CT = Tyler #20; b) TT = Tyler #200
Note: T0 = Control. [a, b] Different letters indicate a significant difference (Dunnett)

the interaction of starch with the other components in the mix, leading to alterations during the mix formation and expansion (Cruz-Tirado et al., 2017). The densities of C and T treatment ranged from 0.14±0.01 to 0.20±0.01 g cm^{-3} and from 0.13±0.01 to 0.41±0.01 g cm^{-3}, respectively. These values matched the ones for trays produced with grape stem and starch (0.18 to 0.21 g cm^{-3}) (Engel et al., 2019) and with ground coffee and starch (0.26 to 0.34 g cm^{-3}) (Trongchuen et al., 2018). The densities were higher than those of trays from cassava residues and biocomposites (0.016 to 0.033 g cm^{-3}) (Engel et al., 2021). There was no noticeable tendency with density due to variation in starch and flour content. CPF slightly increased density, more noticeably in C treatments. If the T treatment particle size was similar when mixed with starch, air capsules may have been reduced during expansion (Bergel et al., 2018). Foam density is critical, as it is indirectly correlated with the mixture expansion capacity (Meng et al., 2019).

Moisture and water absorption

Sample moisture ranged between 3.22% and 6.16%, with 6.24% recorded for the control (Figure 8). The variability in sample moisture was attributed to differences in the proportions of potato peel and CPF, which may be explained by variations in thermoforming time. Cellulose fiber agglomeration and incomplete dispersion induce moisture variations (Peng et al., 2022). Water absorption was reported between 39.10 and 94.07 g of water g^{-1} in C samples and between 32.86 and 92.93 g of water g^{-1} in T samples. Higher fiber concentration (from potato peel and CPF) correlated with lower water absorption, as reported by Cruz-Tirado et al. (2020). Parra-Campos et al. (2022) highlighted the important role of peel cellulose content, particle size, and affinity.

Statistical analysis

Multiple linear regression

Multiple linear regression analysis (Table 2) revealed that trays designed with CPF of Mesh

Table 2. Multiple linear regression

Dependent variable	Regression equation	R^2 (%)	R^2 aj (%)	*p*-value
	Particle size: Mesh #20 CT			
Tensile strength	5.63 - 0.0252 PPS - 0.2198 CPF	51.20	47.58	0.000*
Compression strength	-3.46 + 0.1004 PPS - 0.0806 CPF	70.28	68.07	0.000*
L*	50.38 + 0.168 PPS - 1.425 CPF	72.81	70.12	0.000*
a*	9.16 - 0.1157 PPS + 0.1878 CPF	79.00	77.45	0.000*
b*	29.32 - 0.2963 PPS + 0.0459 CPF	51.43	47.83	0.000*
ΔE	53.43 + 0.141 PPS - 1.425 CPF	72.48	70.45	0.000*
Thickness	0.575 + 0.0350 PPS - 0.0243 CPF	26.06	22.73	0.012*
Moisture	3.58 + 0.0334 PPS - 0.0169 CPF	8.58	1.81	0.298
Water absorption	23.9 + 1.191 PPS - 2.618 CPF	49.46	45.72	0.000*
Density	0.292 - 0.00209 PPS + 0.00891 CPF	15.16	8.87	0.109
	Particle size: Mesh #200 TT			
Tensile strength	1.56 + 0.0230 PPS - 0.1123 CPF	52.33	48.80	0.000*
Compression strength	-3.46 + 0.1004 PPS - 0.0806 CPF	70.28	68.07	0.000*
L*	8.8 + 0.802 PPS - 1.437 CPF	72.22	70.16	0.000*
a*	12.06 - 0.1489 PPS + 0.1159 CPF	60.74	57.83	0.000*
b*	24.61 - 0.2270 PPS - 0.251 CPF	28.01	22.68	0.012*
ΔE	14.3 + 0.734 PPS - 1.467 CPF	74.13	72.22	0.012*
Thickness	0.575 + 0.0350 PPS - 0.0243 CPF	28.06	22.73	0.012*
Moisture	-4.23 + 0.1591 PPS + 0.0425 CPF	60.91	58.01	0.000*
Water absorption	81.7 - 0.025 PPS - 1.68 CPF	7.37	0.51	0.356
Density	0.292 - 0.00209 PPS + 0.00891 CPF	15.16	8.87	0.109

Note: * Significant at $p < 0.05$. PPS = Potato peel starch; PPF = Potato peel flour; CPF = Coffee pulp fiber

#20 particle size (CT) exhibited negative effects on their physical properties, including compression strength and colorimetric parameters (L*, a*, and ΔE). In contrast, trays designed with CPF of Mesh #200 particle size (TT) showed no negative effects on the color parameter a*, unlike CT.

Pareto diagram of standardized effects

The Pareto chart of standardized effects (Figure 9) shows the variables that affected the characteristics of the edible tray. As shown, there were similar effects for both particle sizes (CT and TT). The addition of CPF directly affected tensile strength, L*, a*, and ΔE in both CT and TT. The addition of PPS influenced compression strength, a*, b*, thickness, moisture, and water absorption in both CT and TT. Individually, CPF impacted b* and density in TT, and PPS impacted L*, ΔE, moisture content, water absorption, and density in TT.

Principal components analysis (PCA)

Particle size: Mesh #20 CT

Based on Figure 10a, PC1 accounts for 48.60% of the variance and defines the effect of CPF-CT incorporation. The negative region (left) displays a strong clustering of vectors related to mechanical integrity (compression and tension strength) and L*. Conversely, the positive region (right) indicates that color vectors a* and b* increase with CPF-CT pigmentation, showing an inverse correlation with mechanical strength (compression). Therefore, the shift along the horizontal axis describes a transition from "structural material" to "pigmented composite material".

As shown in Figure 10a, PC2 accounts for 17.90% of the variance and differentiates density behavior. In the positive region (top), the density vector dominates this quadrant, exhibiting its own direction and remaining nearly perpendicular to the color vectors. This suggests that densification is a physical phenomenon independent of pigmentation. The density vector (top right) is almost diametrically opposed to the tensile strength vector (bottom left). This geometric arrangement demonstrates a trade-off in the material: specifically, formulations that achieve higher compaction due to increased density tend to sacrifice their tensile strength.

Particle size: Mesh #200 TT

The analysis of the data matrix for TT reduced the system's dimensionality, explaining 70.24% of the total variance through the first two components. The plot structure reveals a material physics distinct from that observed with CPF-CT. According to Figure 10b, PC1 (horizontal axis)

Particle size: Mesh #20 CT

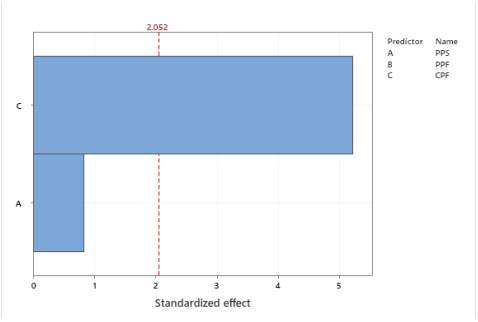

Particle size: Mesh #200 TT

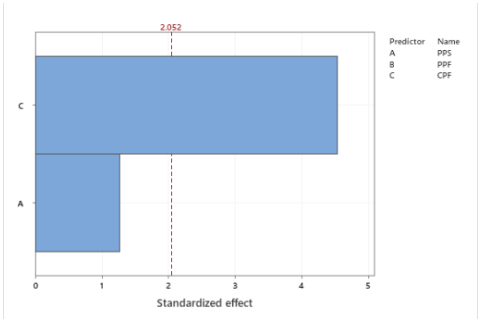

Tensile strength

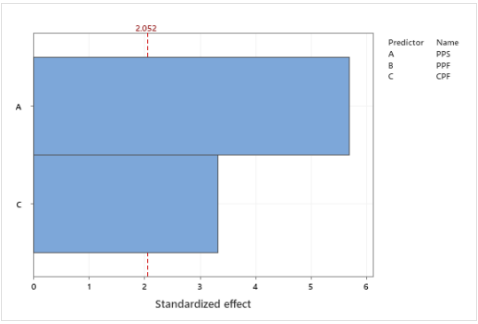

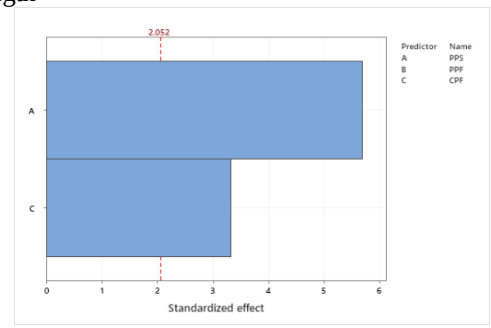

Compression strength

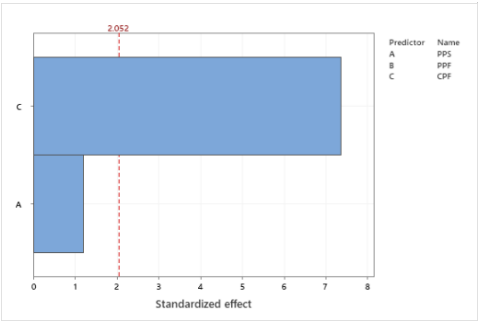

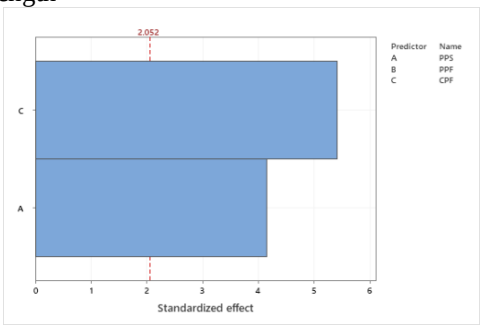

L*

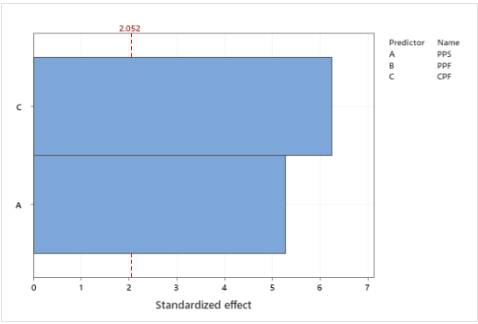

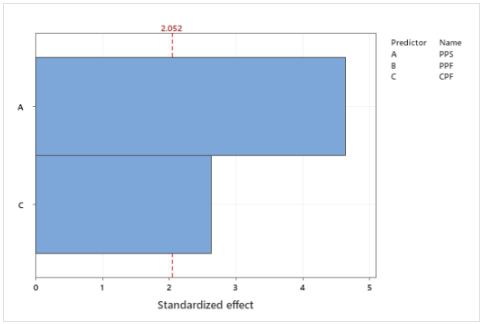

a*

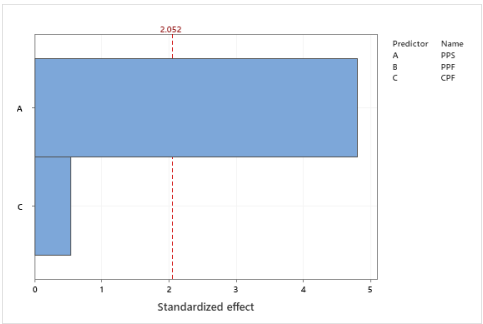

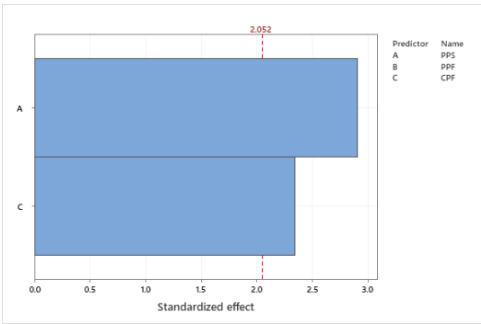

b*

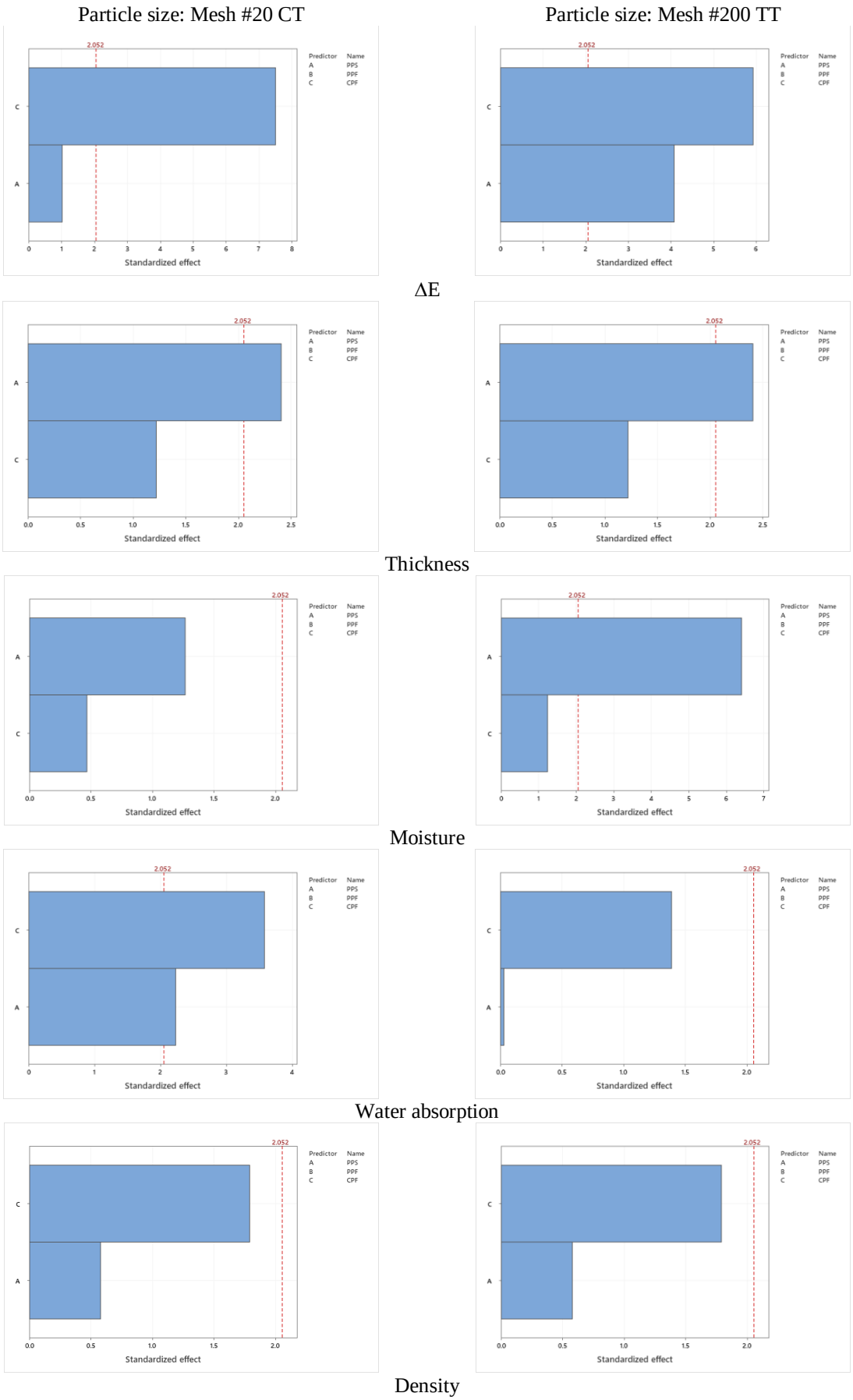

Figure 9. Pareto diagram of standardized effects in tensile, compression, L*, a*, b*, ΔE, thickness, moisture, water absorption, and density

accounts for 53.74% of the variance and describes the primary effect of CPF-TT addition, representing structural integrity vs. fiber loading gradient. This component is the most significant and separates pure, high-strength materials from colored composite materials. PC2 (vertical axis) explains 16.50% and represents the impermeable densification phenomenon. Unlike the previous case, this axis describes a critical competition between density and water absorption.

On PC1, the compression strength, tensile strength, and L* vectors are projected onto the same side of the plot, showing directional clustering. This indicates that the lighter and "purer" samples are consistently the strongest. It is observed that the a* color vector (redness component) projects in the diametrically opposite direction to the mechanical properties. This vector opposition visually confirms that increasing the CPF-TT concentration degrades the mechanical properties of the matrix.

The vertical axis (PC2) reveals a critical physical phenomenon that distinguishes TT from other reinforcements. The density-water antagonism indicates that the density and water absorption vectors point in opposite directions along the vertical axis, forming an angle of nearly 180°. This geometric configuration demonstrates that, for this material, density acts as a direct barrier mechanism. Formulations projecting into the "high density" region are inherently distanced from the "high absorption" zone, confirming an improvement in impermeability through compaction.

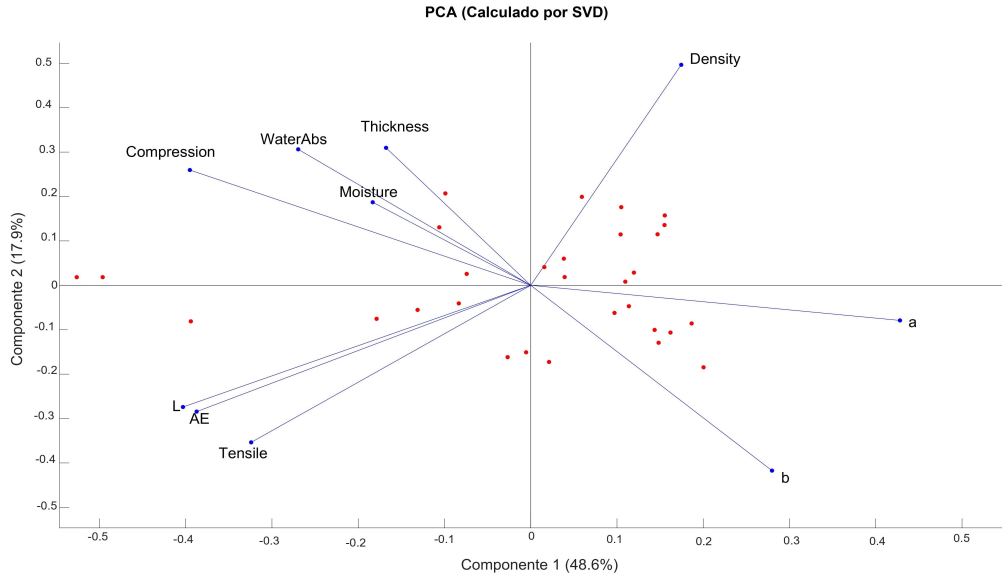

a.

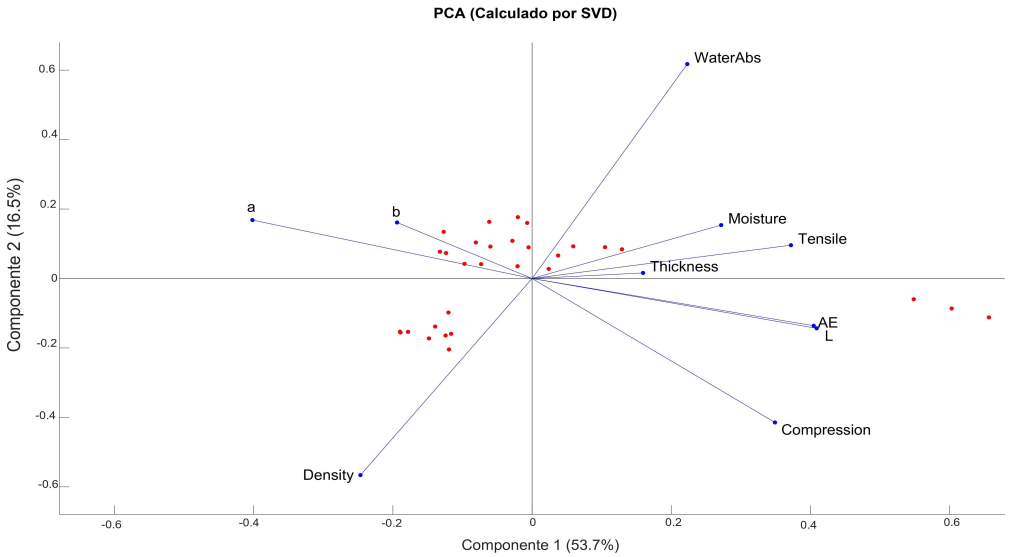

b.

Figure 10. Biplot PCA for the trays CT (a) and TT (b)

Identification of material profiles (clusters)

Particle size: Mesh #20 CT

The distribution of the experimental points across the plane validates three distinct behaviors. The first is the control group (left quadrant), which contains no fiber and exhibits the highest mechanical performance (points associated with compression/tension vectors), as well as a high affinity with the water absorption vector (upper left quadrant), confirming its hydrophilic nature. A second, reinforced group (right quadrant) consists of formulations with high CPF-CT content located in the direction of the color and density vectors, confirming that the fiber acts as a densifying agent and contributes to aesthetic changes. The analysis confirms that the incorporation of CPF-CT alters the polymer matrix, generating denser and visually distinct materials, as indicated by the rightward and upward shift in the plot. However, this structural change leads to a systematic decrease in mechanical tensile and compressive properties, indicated by the leftward shift.

Particle size: Mesh #200 TT

Three distinct zones are defined. The first is designated "high strength," where fiber-free samples are located at the end of the horizontal axis associated with tensile and compressive strength. However, their position also indicates proximity to the influence of moisture vectors, confirming their hydrophilic nature (high water absorption). The second zone is termed "optimal packing," where a specific clustering of formulations with 10% CPF-TT is observed in the region dominated by the density vector. Visually, this group is further removed from the water absorption vector. This suggests that 10% CPF-TT efficiently fills voids within the matrix, maximizing compaction while minimizing water absorption. Subsequently, a third zone, called "saturation," shows that as the fiber dosage increases to 15%, samples shift back toward regions of higher water affinity and lower density, suggesting that excess CPF-TT generates defects or agglomerations that "open" the material's structure. The biplot confirms that the incorporation of CPF-TT introduces a trade-off between mechanical strength and impermeability. Based on these statistical analyses, the tray with the lowest CPF-CT proportion (2.5%) and the tray with a medium CPF-TT content (7.5%) were selected.

Best treatments analysis

Considering that the goal of this research was to design edible trays, CT1 and TT8 treatments were selected based on mechanical and physical test results. The following results were obtained for both treatments. Two texture tests were performed to simulate chewing: the Guillotine test and the biting simulation test, along with a sound emission analysis.

Guillotine test

Two variables were measured: work of shear (toughness) and firmness (Table 3). The CT1 treatment showed lower toughness and firmness than TT8, due to smaller CPF particles in TT8, which provided greater chewing resistance. Both results were superior compared to extruded snacks (6.50 to 30.50 N mm^{-1}) (Ferraz et al., 2019) and highly similar compared to cookies (11.00 to 28.56 N mm^{-1}) (Apaza Fabian and Izquierdo Pantigoso, 2017).

Crunchiness test

Sound emission analysis indicated a significantly higher crunchiness for CT1 (76.97±0.66 dB) than for TT8 (73.95±0.16 dB) ($p < 0.05$). Higher crunchiness has been related to starch content (Cruz-Tirado et al., 2017), yet it is also associated with a weaker tray structure, which in turn, is related to higher loss during unmolding, packing, and distribution. These 2 tests shed light on key information to characterize tray resistance.

Biting simulation test

Unlike the previous test, the biting simulation test simulated a tooth, yet the observed variable was firmness. The firmness of TT8 (858.22±75.08 g) was significantly higher than that of CT1

Table 3. Crunchiness and mechanical analyses

Sample	Guillotine test			Biting simulation test	
	Toughness (N mm^{-2})	Firmness (N mm^{-1})	Sound (dB)	Firmness (g)	Sound (dB)
CT1	8.81±0.47[a]	10.37±1.14[a]	76.97±0.66[a]	547.19±8.97[a]	68.22±0.38[a]
TT8	12.13±1.08[b]	12.79±1.54[b]	73.95±0.16[b]	858.22±75.08[b]	67.63±0.22[b]

Note: [a, b] Different letters in row indicate a significant difference (Dunnett); CT = Tyler #20; TT = Tyler #200

(547.19±38.97 g) ($p < 0.05$). However, the sound emission recorded was significantly higher for CT1 (68.22±0.38 dB) than for TT8 (67.63±0.22 dB) ($p < 0.05$). Guillotine and biting simulation tests showed similar results, indicating TT8 as the best treatment. Due to its composition, TT8 showed a lower starch and higher fiber content (potato peel and coffee pulp), resulting in a more compact structure. As such, higher firmness or toughness was related to a less crunchy sound.

Fourier-transform infrared spectroscopy (FTIR)

Figure 11 shows the FTIR spectra for the two main treatments (CT1 and TT8), illustrating interactions between PPS, PPF, and CPF. Similar peaks with vertical shifts were linked to the sample composition. A reduction in the 3,500 to 3,000 cm^{-1} bands, corresponding to the hydroxyl group, compared with CT1, indicated that potato peel and CPF were present on the foam surface and that TT8 contained a lower starch content (Bergel et al., 2018). The 3,000 to 2,900 cm^{-1} band was linked to the stretching of C–H bonds; the 1,400 to 1,300 cm^{-1} band was linked to the symmetrical and asymmetrical vibrations of C–H bonds. While the 1,200 to 1,000 cm^{-1} band showed peaks typical of starch and other polysaccharides (fiber, cellulose, etc.) and was linked to the acetal (C–O–C) group vibrations (Lima et al., 2012; Wokadala et al., 2014). The 1,750 to 1,700 cm^{-1} band was linked to the stretching of the carbonyl C=O group due to interactions between starch and added polysaccharides (Bergel et al., 2018). Trongchuen et al. (2017) demonstrated that combining starch with other substances may result in their degradation with heat.

Scanning electron microscopy (SEM)

SEM images of CT1 and TT8 showed the internal structures in a cross-section of the trays (Figure 12). Both treatments showed a porous transverse section, possibly due to the quick water evaporation during molding, leading to bubble rupture (Cinelli et al., 2006). However, TT8 showed a more compact structure with smaller air bubbles, probably due to a higher fiber content and lower CPF particles. This finding is consistent with Cruz-Tirado et al. (2020), who reported that increased fiber content reduces overall internal porosity. Moreover, as reported by Cruz-Tirado et al. (2020), higher starch content was associated with bigger internal bubbles.

Edible tray nutritional value

The nutritional value of the edible tray turned out to be low (16 to 19% of the recommended daily intake), with mainly carbohydrates (85.96

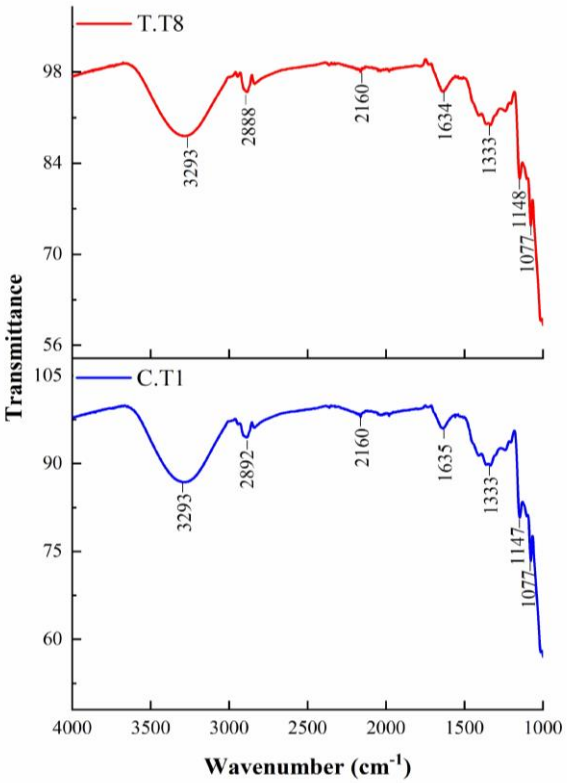

Figure 11. FTIR spectra of CT1 and TT8

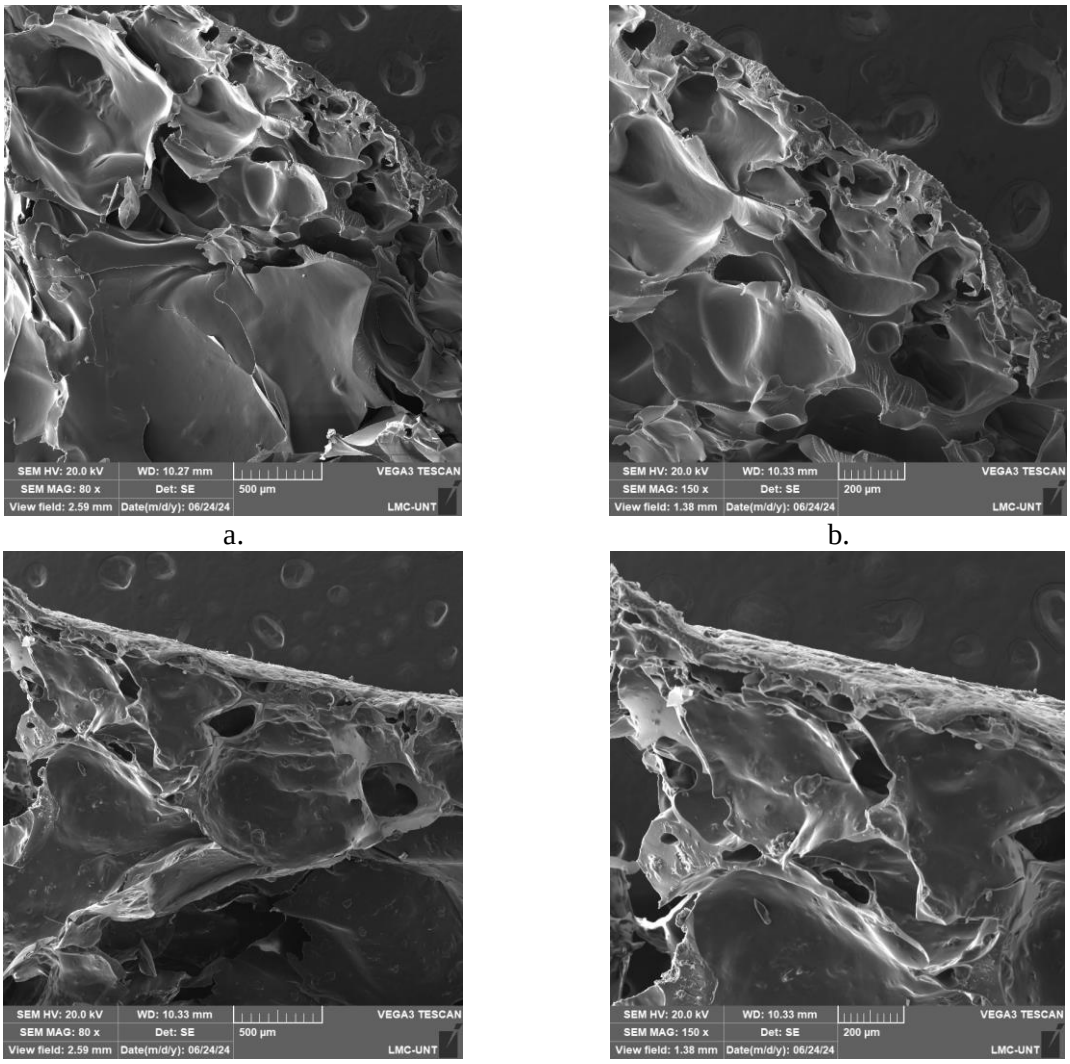

Figure 12. Edible tray SEM micrographs: a) CT1, 80× resolution; b) CT1, 150× resolution; c) TT8, 80× resolution; d) TT8, 150× resolution

Table 4. Edible tray nutritional value

Component	Protein	Fat	Fiber	Carbohydrates	Energy	Iron	Zinc	Magnesium
	g 100 g^{-1}				kcal	mg kg^{-1}		
CT1	1.17	1.78	3.07	85.96	315.00	44.90	18.66	3.47
TT8	1.02	2.19	3.44	92.60	376.50	56.70	16.52	3.89

Table 5. Iron bioaccessibility (mg kg^{-1}) in edible trays

Sample	Mouth	Stomach	Small intestine
CT1	0.93±0.15	1.22±0.20	1.28±0.01
TT8	1.13±0.10	1.69±0.07	1.81±0.05

to 92.60%) and fiber (3.07 to 3.44%). Regarding the iron content from CPF, it stood out (44.90 to 56.70 mg kg^{-1}) (Table 4). TT8 showed a higher iron bioavailability (1.13 to 1.81 mg kg^{-1}) compared with CT1 (0.93 to 1.28 mg kg^{-1}) ($p < 0.05$) (Table 5). The bioaccessibility of iron in edible trays was much lower than in the bean extract (67.4 mg kg^{-1}) but higher than in textured peas (0.5 mg kg^{-1}) (Auer et al., 2024). Iron bioavailability tended to increase as the samples progressed from the mouth to the small intestine. The high fiber content from potato peel and coffee pulp likely formed an egg carton-like structure, which increased iron bioavailability in TT8 until reaching the small intestine (Durán et al., 2017).

CONCLUSIONS

This study demonstrated the feasibility of utilizing CPF and potato peel residues as reinforcement materials to produce edible trays from "Huevo de Indio" potato starch through a thermocompression molding process. PCA successfully elucidated the distinct physical behaviors induced by the incorporation of CPF. For both coarse (CPF-CT) and thin (CPF-TT) fibers, the first two components accounted for over 70% of the total variance. Based on this multidimensional analysis, formulations with 2.5% (CT1) and 7.5% (TT8) were identified as optimal candidates, as they maintained sufficient structural performance while achieving the densification required for food-grade edible trays. The resulting trays exhibited a favorable appearance, adequate expansion, and a homogeneous fiber distribution within the polymer matrix. Specifically, the PPS/PPF/CPF ratios of 60 g/5 g/2.5 g (CT1) and 50 g/15 g/7.5 g (TT8) showed superior CPF dispersion, density, and water absorption balance. Results from guillotine and bite simulation tests, FTIR, SEM, nutritional analysis, and iron bioaccessibility confirmed that TT8 possessed the best overall qualities. Future research should focus on determining the shelf life of the edible trays and investigating methods to further enhance iron bioavailability.

ACKNOWLEDGEMENT

The CONCYTEC-World Bank Project provided funding for the iron bioaccessibility analysis conducted at the CONACYT Public Research Centre in Jalisco, Mexico, uunder Contract 008-2018-FONDECYT-BM-IADT-MU. The authors would also like to express their gratitude to Eng. Hernán Alvarado Quintana, Director of the Ceramic Materials Laboratory at UNT, Materials Engineering, for his assistance in capturing SEM images.

REFERENCES

Abera, G., Woldeyes, B., Dessalegn Demash, H., & Miyake, G. M. (2019). Comparison of physicochemical properties of indigenous Ethiopian tuber crop (*Coccinia abyssinica*) starch with commercially available potato and wheat starches. *International Journal of Biological Macromolecules*, *140*, 43–48. https://doi.org/10.1016/j.ijbiomac.2019.08.118

Aguirre, E., Domínguez, J., Villanueva, E., Ponce-Ramirez, J. A., de Fátima Arevalo-Oliva, M., Siche, R., ... & Rodríguez, G. (2023). Biodegradable trays based on *Manihot esculenta* Crantz starch and *Zea mays* husk flour. *Food Packaging and Shelf Life*, *38*, 101129. https://doi.org/10.1016/j.fpsl.2023.101129

Akter, M., Anjum, N., Roy, F., Yasmin, S., Sohany, M., & Mahomud, M. S. (2023). Effect of drying methods on physicochemical, antioxidant and functional properties of potato peel flour and quality evaluation of potato peel composite cake. *Journal of Agriculture and Food Research*, *11*, 100508. https://doi.org/10.1016/j.jafr.2023.100508

Alvis, A., Vélez, C. A., Villada, H. S., & Rada-Mendoza, M. (2008). Análisis físico-químico y morfológico de almidones de ñame, yuca y papa y determinación de la viscosidad de las pastas. *Información Tecnológica*, *19*(1), 19–28. https://doi.org/10.4067/S0718-07642008000100004

AOAC. (2019). *Official Methods of Analysis*. Association of Official Analitical Chemists. Retrieved from http://eoma.aoac.org/app_d.pdf

Apaza Fabian, K. D., & Izquierdo Pantigoso, Y. P. (2017). *Valor nutritivo y aceptabilidad de la fortificación de galletas a base de harina de trigo (Triticum aestivum), harina de tarwi (Lupinus mutabilis) y bazo de res, para escolares, Arequipa 2017*. Retrieved from http://repositorio.unsa.edu.pe/handle/UNSA/4669

Auer, J., Alminger, M., Marinea, M., Johansson, M., Zamaratskaia, G., Högberg, A., & Langton, M. (2024). Assessing the digestibility and estimated bioavailability/bioaccessibility of plant-based proteins and minerals from soy, pea, and faba bean ingredients. *Lwt*, *197*, 115893. https://doi.org/10.1016/j.lwt.2024.115893

Ayala, R. Y., Meléndez-Mori, J. B., Haro, N., Vilca Valqui, N. C., & Oliva-Cruz, M. (2025). Perception of climate change among smallholder potato producers in northern Peru. *Sustainable Environment*, *11*(1), 2521945. https://doi.org/10.1080/27658511.2025.2521945

Bardales, Á. D. N., Garay, S. G. M., Tiburcio, J. E. V., Portal, R. M. R., Gómez, R. E. C.,

Rosales, C. R. C., ... & Aguilar, A. M. (2022). Caracterización fisicoquímica de cuatro variedades de papas nativas (*Solanum tuberosum*) con aptitud para fritura, cultivadas en dos zonas en Huánuco. *Revista de La Sociedad Química Del Perú*, *88*(3), 237–250. http://dx.doi.org/10.37761/rsqp.v88i3.400

Bergel, B. F., Osorio, S. D., da Luz, L. M., & Santana, R. M. C. (2018). Effects of hydrophobized starches on thermoplastic starch foams made from potato starch. *Carbohydrate Polymers*, *200*, 106–114. https://doi.org/10.1016/j.carbpol.2018.07.047

Bollamma, P. B. K., Nanjamma, K. K., & Ponnappa, K. C. (2023). Coffee pulp: From a by-product of coffee production to a potential anticariogenic mouth rinse! An *in vivo* study. *Journal of Conservative Dentistry and Endodontics*, *26*(6), 693–696. https://doi.org/10.4103/JCDE.JCDE_149_23

Charles, M., Endrizzi, I., Aprea, E., Zambanini, J., Betta, E., & Gasperi, F. (2017). Dynamic and static sensory methods to study the role of aroma on taste and texture: A multisensory approach to apple perception. *Food Quality and Preference*, *62*, 17–30. https://doi.org/10.1016/j.foodqual.2017.06.014

Chen, Y., Awasthi, A. K., Wei, F., Tan, Q., & Li, J. (2021). Single-use plastics: Production, usage, disposal, and adverse impacts. *Science of the Total Environment*, *752*, 141772. https://doi.org/10.1016/j.scitotenv.2020.141772

Cinelli, P., Chiellini, E., Lawton, J. W., & Imam, S. H. (2006). Foamed articles based on potato starch, corn fibers and poly (vinyl alcohol). *Polymer Degradation and Stability*, *91*(5), 1147–1155. https://doi.org/10.1016/j.polymdegradstab.2005.07.001

Collazos, C., Alvisur, E., Vásquez, J., Herrera, N., Robles, N., Arias, M., … & Días, C. (1996). *Tablas peruanas de composición de alimentos*. Instituto Nacional de Salud, Lima (Peru); Centro Nacional de Alimentación, Nutrición y Vida Saludable (CENAN). Retrieved from https://lamejorreceta.ins.gob.pe/sites/default/files/2020-12/tablas-peruanas-QR_0.pdf

Cruz-Tirado, J. P., Barros Ferreira, R. S., Lizárraga, E., Tapia-Blácido, D. R., Silva, N. C. C., Angelats-Silva, L., & Siche, R. (2020). Bioactive Andean sweet potato starch-based foam incorporated with oregano or thyme essential oil. *Food Packaging and Shelf Life*, *23*, 100457. https://doi.org/10.1016/j.fpsl.2019.100457

Cruz-Tirado, J. P., Tapia-Blácido, D. R., & Siche, R. (2017). Influence of proportion and size of sugarcane bagasse fiber on the properties of sweet potato starch foams. *IOP Conference Series: Materials Science and Engineering*, *225*, 012180. https://doi.org/10.1088/1757-899X/225/1/012180

Devidas Meshram, B., Kisanrao Lule, V., Vyawahare, S., & Rani, R. (2023). Application of edible packaging in dairy and food industry. *Food processing and packaging technologies - Recent advances*. IntechOpen. https://doi.org/10.5772/intechopen.107850

Duangjai, A., Suphrom, N., Wungrath, J., Ontawong, A., Nuengchamnong, N., & Yosboonruang, A. (2016). Comparison of antioxidants, antimicrobial activities and chemical profiles of three coffee (*Coffea arabica* L.) pulp aqueous extracts. *Integrative Medicine Research*, *5*(4), 324–331. https://doi.org/10.1016/j.imr.2016.09.001

Durán, E., Villalobos, C., Churio, O., Pizarro, F., & Valenzuela, C. (2017). Encapsulación de hierro: Otra estrategia para la prevención o tratamiento de la anemia por deficiencia de hierro. *Revista Chilena de Nutrición*, *44*(3), 234–243. http://dx.doi.org/10.4067/s0717-75182017000300234

Dybka-Stępień, K., Antolak, H., Kmiotek, M., Piechota, D., & Koziróg, A. (2021). Disposable food packaging and serving materials—Trends and biodegradability. *Polymers*, *13*(20), 3606. https://doi.org/10.3390/polym13203606

Elfaleh, I., Abbassi, F., Habibi, M., Ahmad, F., Guedri, M., Nasri, M., & Garnier, C. (2023). A comprehensive review of natural fibers and their composites: An eco-friendly alternative to conventional materials. *Results in Engineering*, *19*, 101271. https://doi.org/10.1016/j.rineng.2023.101271

Engel, J. B., Ambrosi, A., & Tessaro, I. C. (2019). Development of biodegradable starch-based foams incorporated with grape stalks for food packaging. *Carbohydrate Polymers*, *225*, 115234. https://doi.org/10.1016/j.carbpol.2019.115234

Engel, J. B., Luchese, C. L., & Tessaro, I. C. (2021). How are the properties of biocomposite foams influenced by the substitution of cassava starch for its residual sources? *Food Hydrocolloids, 118*, 106790. https://doi.org/10.1016/j.foodhyd.2021.106790

Ferraz, C. A., Fontes, R. L. S., Fontes-Sant'Ana, G. C., Calado, V., López, E. O., & Rocha-Leão, M. H. M. (2019). Extraction, modification, and chemical, thermal and morphological characterization of starch from the agro-industrial residue of mango (*Mangifera indica* L) var. Ubá. *Starch-Stärke*, *71*(1–2), 1800023. https://doi.org/10.1002/star.201800023

Habibi, M., Selmi, S., Laperrière, L., Mahi, H., & Kelouwani, S. (2020). Damage analysis of low-velocity impact of non-woven flax epoxy composites. *Journal of Natural Fibers*, *17*(11), 1545–1554. https://doi.org/10.1080/15440478.2019.1584076

Kahvand, F., & Fasihi, M. (2020). Microstructure and physical properties of thermoplastic corn starch foams as influenced by polyvinyl alcohol and plasticizer contents. *International Journal of Biological Macromolecules*, *157*, 359–367. https://doi.org/10.1016/j.ijbiomac.2020.04.222

Khan, S., Hashim, S. B., Arslan, M., Zhang, K., Bilal, M., Zhiyang, C., ... & Zou, X. (2024). Berry wax improves the physico-mechanical, thermal, water barrier properties and biodegradable potential of chitosan food packaging film. *International Journal of Biological Macromolecules*, *261*, 129821. https://doi.org/10.1016/j.ijbiomac.2024.129821

Leya, B., Franklin, R. S., Pragalyaashree, M. M., Monicka, A. A., Tiroutchelvame, D., Blessy, C., & Blessie, R. F. (2024). Biopolymer-based edible packaging: A critical review on biomaterials, formation, and applications on food products. *Journal of Applied Biology & Biotechnology*, *12*(6), 42–57. https://doi.org/10.7324/JABB.2024.145531

Lima, B. N. B., Cabral, T. B., C Neto, R. P., Tavares, M. I. B., & Pierucci, A. P. T. (2012). Estudo do amido de farinhas comerciais comestíveis. *Polímeros*, *22*, 486–490. https://doi.org/10.1590/S0104-14282012005000062

Lin, C.-L., Lin, J.-H., Lin, J.-J., & Chang, Y.-H. (2020). Properties of high-swelling native starch treated by heat–moisture treatment with different holding times and iterations. *Molecules*, *25*(23), 5528. https://doi.org/10.3390/molecules25235528

Mao, Y., Li, H., Gu, W., Yang, G., Liu, Y., & He, Q. (2020). Distribution and characteristics of microplastics in the Yulin River, China: Role of environmental and spatial factors. *Environmental Pollution*, *265*, 115033. https://doi.org/10.1016/j.envpol.2020.115033

Martínez, P., Betalleluz-Pallardel, I., Cuba, A., Peña, F., Cervantes-Uc, J. M., Uribe-Calderón, J. A., & Velezmoro, C. (2022). Effects of natural freeze-thaw treatment on structural, functional, and rheological characteristics of starches isolated from three bitter potato cultivars from the Andean region. *Food Hydrocolloids*, *132*, 107860. https://doi.org/10.1016/j.foodhyd.2022.107860

Meng, L., Liu, H., Yu, L., Duan, Q., Chen, L., Liu, F., ... & Lin, X. (2019). How water acts as both blowing agent and plasticizer affect starch-based foam. *Industrial Crops and Products*, *134*, 43–49. https://doi.org/10.1016/j.indcrop.2019.03.056

Mohareb, E., & Mittal, G. S. (2007). Formulation and process conditions for biodegradable/edible soy-based packaging trays. *Packaging Technology and Science: An International Journal*, *20*(1), 1–15. https://doi.org/10.1002/pts.736

Morrison, W. R., & Laignelet, B. (1983). An improved colorimetric procedure for determining apparent and total amylose in cereal and other starches. *Journal of Cereal Science*, *1*(1), 9–20. https://doi.org/10.1016/S0733-5210(83)80004-6

Moustafa, M., A. Abu-Saied, M., H. Taha, T., Elnouby, M., A. El Desouky, E., Alamri, S., ... & Al-Emam, A. (2021). Preparation and characterization of super-absorbing gel formulated from κ-carrageenan–potato peel starch blended polymers. *Polymers*, *13*(24), 4308. https://doi.org/10.3390/polym13244308

Namphonsane, A., Amornsakchai, T., Chia, C. H., Goh, K. L., Thanawan, S., Wongsagonsup, R., & Smith, S. M. (2023). Development of biodegradable rigid foams from pineapple field waste. *Polymers*, *15*(13), 2895. https://doi.org/10.3390/polym15132895

Oliveira Filho, J. G., & Egea, M. B. (2022). Edible bioactive film with curcumin: A potential "functional" packaging? *International Journal of Molecular Sciences*, *23*(10), 5638. https://doi.org/10.3390/ijms23105638

Olivera, D. F., & Salvadori, V. O. (2011). Instrumental and sensory evaluation of cooked pasta during frozen storage. *International Journal of Food Science & Technology*, *46*(7), 1445–1454. https://doi.org/10.1111/j.1365-2621.2011.02638.x

Osorio Mora, O., Ceron Cardenas, A. F., & Bucheli, M. A. (2014). Elaboración de galletas a base de harina de papa de la variedad parda pastusa (*Solanum tuberosum*). *Acta Agronómica*, *63*(2), 101–109. https://doi.org/10.15446/acag.v63n2.39575

Pandiselvam, R., Mitharwal, S., Rani, P., Shanker, M. A., Kumar, A., Aslam, R., ... & Khaneghah, A. M. (2023). The influence of non-thermal technologies on color pigments of food materials: An updatedreview. *Current Research in Food Science*, *6*, 100529. https://doi.org/10.1016/j.crfs.2023.100529

Parra-Campos, A., Serna-Cock, L., & Solanilla-Duque, J. F. (2022). Effect of the addition of fique bagasse microparticles in obtaining a biobased material based on cassava starch. *International Journal of Biological Macromolecules*, *207*, 289–298. https://doi.org/10.1016/j.ijbiomac.2022.03.016

Patel, P. (2019). Edible packaging. *ACS Central Science*, *5*(12), 1907–1910. https://doi.org/10.1021/acscentsci.9b01251

Peng, S., Li, F., Man, J., Li, J., Zhang, C., Ji, M., ... & Wang, S. (2022). Enhancing the properties of starch-fiber foaming material by adjusting fiber length: The synergistic effect of macro-micro stress conduction. *Materials Today Communications*, *33*, 104408. https://doi.org/10.1016/j.mtcomm.2022.104408

Quispe-Sanchez, L., Chuquilín-Goicochea, R., Figueroa-Avalos, H. M., Chavez, S. G., Yoplac, I., Mori, S., ... & Oliva-Cruz, M. (2025). Biodegradable trays of cassava starch reinforced with Ceiba, coffee and cocoa fibers: A sustainable alternative to plastics. *Applied Food Research*, *5*(2), 101277. https://doi.org/10.1016/j.afres.2025.101277

Rawangkan, A., Siriphap, A., Yosboonruang, A., Kiddee, A., Pook-In, G., Saokaew, S., ... & Duangjai, A. (2022). Potential antimicrobial properties of coffee beans and coffee by-products against drug-resistant *Vibrio cholerae*. *Frontiers in Nutrition*, *9*, 865684. https://doi.org/10.3389/fnut.2022.865684

Rodrigues, D. B., Marques, M. C., Hacke, A., Loubet Filho, P. S., Cazarin, C. B. B., & Mariutti, L. R. B. (2022). Trust your gut: Bioavailability and bioaccessibility of dietary compounds. *Current Research in Food Science*, *5*, 228–233. https://doi.org/10.1016/j.crfs.2022.01.002

Rondon-Jara, E., Lipa-Echevarría, K., Marchena-Barrientos, S., Chambi-Quispe, M. L., & Carocancha-Condori, G. J. (2020). Comparación de las leyes sobre el consumo de bolsas plásticas en Perú y Chile. *Producción+ Limpia*, *15*(2), 175–187. https://doi.org/10.22507/pml.v15n2a9

Sampaio, S. L., Petropoulos, S. A., Alexopoulos, A., Heleno, S. A., Santos-Buelga, C., Barros, L., & Ferreira, I. C. F. R. (2020). Potato peels as sources of functional compounds for the food industry: A review. *Trends in Food Science & Technology*, *103*(1), 118–129. https://doi.org/10.1016/j.tifs.2020.07.015

Tokumura, C., & Mejía, E. (2023). Anemia infantil en el Perú: En el baúl de los pendientes. *Revista Médica Herediana*, *34*(1), 3–4. http://dx.doi.org/10.20453/rmh.v34i1.4445

Trongchuen, K., Ounkaew, A., Kasemsiri, P., Hiziroglu, S., Mongkolthanaruk, W., Wannasutta, R., ... & Chindaprasirt, P. (2018). Bioactive starch foam composite enriched with natural antioxidants from spent coffee ground and essential oil. *Starch-Stärke*, *70*(7–8), 1700238. https://doi.org/10.1002/star.201700238

Vallejos-Jiménez, A., Cadena-Chamorro, E. M., Santa, J. F., Buitrago-Sierra, R., Dugmore, T. I. J., Bose, S., & Matharu, A. S. (2025). Development of novel pectin-based films from coffee waste: Mucilage and pulp. *Waste and Biomass Valorization*, *16*(10), 5503–5518. https://doi.org/10.1007/s12649-025-02926-9

Wang, S., Chen, H., Zhou, X., Tian, Y., Lin, C., Wang, W., ... & Lin, H. (2020). Microplastic abundance, distribution and composition

in the mid-west Pacific Ocean. *Environmental Pollution*, *264*, 114125. https://doi.org/10.1016/j.envpol.2020.114125

Wokadala, O. C., Emmambux, N. M., & Ray, S. S. (2014). Inducing PLA/starch compatibility through butyl-etherification of waxy and high amylose starch. *Carbohydrate Polymers*, *112*, 216–224. https://doi.org/10.1016/j.carbpol.2014.05.095

Wrolstad, R. E., & Smith, D. E. (2017). Color analysis. *Food Analysis*, pp. 545–555. https://doi.org/10.1007/978-3-031-50643-7_31

Zhang, Y., Diehl, A., Lewandowski, A., Gopalakrishnan, K., & Baker, T. (2020). Removal efficiency of micro-and nanoplastics (180 nm–125 μm) during drinking water treatment. *Science of The Total Environment*, *720*, 137383. https://doi.org/10.1016/j.scitotenv.2020.137383